Deflectometry for ophthalmic optics testing and the impact of test surface orientation

Rebecca Su, Heejoo Choi, Daewook Kim, James Schwiegerling

Rebecca Su, Heejoo Choi, Daewook Kim, James Schwiegerling, "Deflectometry for ophthalmic optics testing and the impact of test surface orientation," Proc. SPIE 12672, Applied Optical Metrology V, 1267206 (4 October 2023); doi: 10.1117/12.2676217

SPIE.

Event: SPIE Optical Engineering + Applications, 2023, San Diego, California, United States

Deflectometry for ophthalmic optics testing and the impact of test surface orientation

Rebecca Su[a], Heejoo Choi*[a,b], Daewook Kim[a,b,c], and James Schwiegerling[a]

[a]Wyant College of Optical Sciences, University of Arizona, 1630 E. University Blvd., Tucson, AZ 85721, USA
[b]Large Binocular Telescope Observatory, University of Arizona, 933 N Cherry Ave., Tucson, AZ 85721, USA
[c]Department of Astronomy and Steward Observatory, University of Arizona, 933 N. Cherry Ave., Tucson, AZ 85721, USA

ABSTRACT

The effects of the misalignment of a test surface in a deflectometry system were explored. A Stewart Platform Hexapod stage was used to create the intentional misalignment, rotate the test surface position around the X and Y axes as well as displace their Z location. The measured surface maps were analyzed in coefficients of a fit of the surface map to the Zernike coefficients. The Zernike term results were adopted to show the relationship between the induced pose changes and the reconstructed surface map. Such an understanding of the errors in location and orientation and deflectometry measurement results would be beneficial in the future measurement of ophthalmic optics with a deflectometry system.

Keywords: optical testing, deflectometry, ophthalmology, misalignment, Stewart Platform

1. INTRODUCTION

The human eye is one of the most complex organs in the human body. However, most of the global population suffers from some type of refractive error. Not only do patients tend to suffer from refractive error in their eyes, as patients age they develop presbyopia which refers to the stiffening in the crystalline lens that prevents the eye from being able to accommodate to view near and far scenes. Currently reading glasses with add power as well as bifocals and even progressive lenses are the most used solutions for addressing presbyopia. Fortunately, recently there have been many exciting developments in presbyopia aids such as multifocal contact lenses and intraocular lenses.[1]

However, as the ophthalmic optics community continues to improve designs of visual aids, there is a corresponding need for metrology systems sophisticated enough to verify the results of these complex surface shapes. Traditional lens verification methods include the usage of lensometers and interferometers.[2] While lensometers are an excellent "in clinic" verification method, they are inconvenient for testing specialty lenses. Lenses such as progressive addition lenses require the clinician to move the lens to various positions to verify the optical power of the different regions. Therefore interferometry and Hartmann-Shack wavefront sensing are also popular methods for verifying optical properties and performance of more complicated ophthalmic lenses.

Interferometric testing requires a null testing setup. With free-form and aspheric surfaces, such a null test surface is difficult to acquire. Computer generated holograms are often used as a null optics for interferometric testing, but they are quite expensive to manufacture[3] and require skillful aligning knowledge. For complex spectacle lenses which are designed to fit a personalized set of user needs, deflectometry would be an exciting alternative to interferometry as it does not require a null testing surface.[4] Additionally, deflectometry has also demonstrated similar surface reconstruction accuracy to commercial interferometric systems.[5]

Further author information: (Send correspondence to H. Choi)
H. Choi: E-mail: hchoi@optics.arizona.edu

Applied Optical Metrology V, edited by Erik Novak, Christopher C. Wilcox, Proc. of SPIE
Vol. 12672, 1267206 · © 2023 SPIE · 0277-786X · doi: 10.1117/12.2676217

Deflectometry is based on the principle of the reverse Hartmann test. Structured light patterns are displayed on a monitor and reflected from the unit under test are captured by a complementary metal oxide semiconductor (CMOS) camera. When using phase-shifting deflectometry, these structured light patterns take the form of four $\pi/2$ phase shifted stripe patterns in both the horizontal and vertical directions. The phase-shifted images are then analyzed using the following arctangent equation (1) to recover both horizontal and vertical phase maps stretching across the surface of the unit under test (UUT).

$$\Phi = arctan\frac{I_4 - I_2}{I_1 - I_3} \tag{1}$$

After recovering vertical and horizontal phase maps of the UUT, the corresponding pixel positions along the monitor surface is determined by matching the phase values on the UUT to the phase values on the monitor. Once this "pixel to pixel" relationship is identified, the vertical and horizontal slopes of the UUT may be calculated through a simple geometric triangulation. This triangle is formed between the three points of interest: the camera location, the surface intersection point, and the monitor intersection point. There are two main assumptions that are necessary for connecting these points. Assuming that light travels in straight lines and undergoes specular reflection at the UUT, the ray path creates an angle between these three points. The normal of the intersection plane bisects this angle. The geometry of the system can be seen in Figure 1. Through this geometry, the vertical and horizontal slope of the UUT can be calculated using Equation 2 and 3.[6] In these equations x_m and y_m refer to the X-coordinate and Y-coordinate intercept locations of the UUT. x_{screen} and y_{screen} refer to the intercept locations of the ray tracing to the monitor. x_{camera} and y_{camera} refer to the starting location of the ray path from the camera. $d_{m2screen}$ and $z_{m2screen}$ are assumed to be equal in these experiments and $Z(x_m,\ y_m)$ is assumed to be 0 initially due to the nature of the flat mirror test surface. Once this position information is used to generate vertical and horizontal slope maps, the surface map is constructed via Southwell Integration.

$$w_x\left(x_m,\ y_m\right) = \frac{\frac{x_m - x_{screen}}{d_{m2screen}} + \frac{x_m - x_{camera}}{d_{m2screen}}}{\frac{z_{m2screen} - Z(x_m,\ y_m)}{d_{m2screen}} + \frac{z_{m2screen} - Z(x_m,\ y_m)}{d_{m2camera}}} \tag{2}$$

$$w_y\left(x_m,\ y_m\right) = \frac{\frac{y_m - y_{screen}}{d_{m2screen}} + \frac{y_m - y_{camera}}{d_{m2screen}}}{\frac{z_{m2screen} - Z(x_m,\ y_m)}{d_{m2screen}} + \frac{z_{m2screen} - Z(x_m,\ y_m)}{d_{m2camera}}} \tag{3}$$

As shown in the equation, the accuracy of the reconstructed surface map depends on the accuracy of the coordinate information of the three points of interest. Since the slope maps are numerically calculated from the knowledge of the position information, this process depends entirely upon accurately understanding the positioning of the UUT. Precisely measuring the relative position of the UUT with respect to the deflectometer is a fundamental requirement for obtaining a reliable surface map. The remainder of this paper will explore the effects of intentionally perturbing the UUT orientation on the deflectometry measurement results in the form of Zernike coefficients.

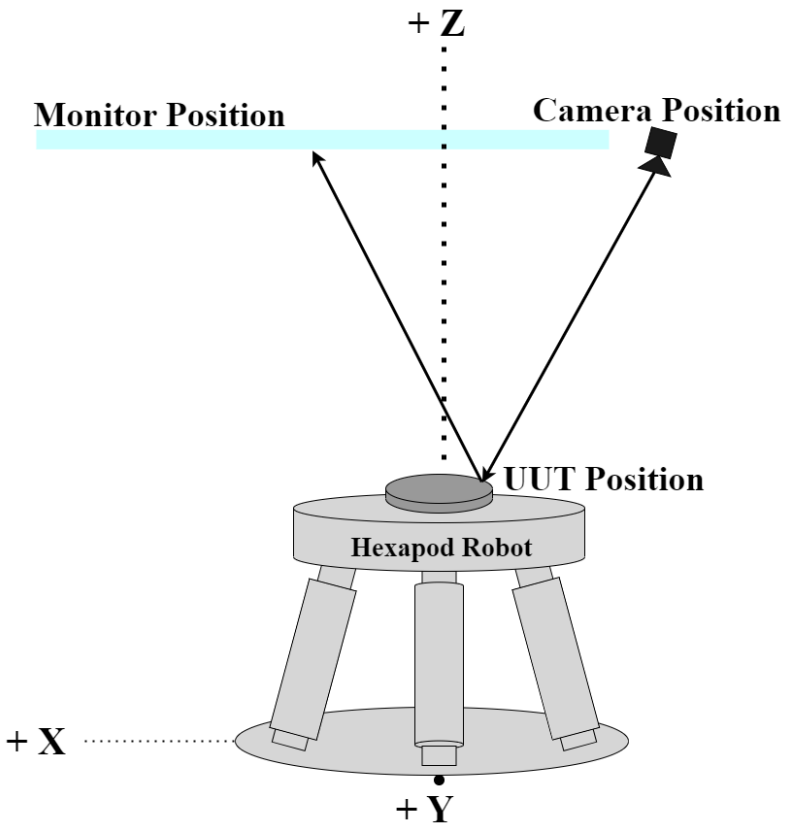

Figure 1. Schematic diagram of deflectometry components with hexapod system.

2. EXPERIMENT

A deflectometry system was constructed consisting of a monitor, a camera, and a hexapod stage as shown in the Figure 2. The hexapod was used as the positioning platform for the UUT, a 75 mm diameter flat mirror. A self-centering jaw clamp mount held the mirror in place. The hexapod stage adjusted the position and orientation from the initial "home" position. Then, the software package SAGUARO (Software Analysis Graphical-user-interface from University of Arizona for Research in Optics)[7] was used to take the raw data measurements and conduct the analysis. Raw data was collected at each perturbed pose without changing the initial input information. The measurement data was then processed, and the surface shape was analyzed through a fitting of the surface map to the first 11 Zernike coefficients as defined by the convention listed in Ansys Zemax OpticStudio's Zernike Standard Coefficients. These coefficients were recorded and subtracted from their counterparts measured when the UUT was positioned at its known position. This generated the residual value Zernike coefficients. Once these residual values were calculated, they were plotted as a function of the UUT perturbation.

2.1 Equipment

The test setup consisted of an ACROME Stewart Pro as the hexapod stage, a 23 inch W-LED Acer H236HL monitor and a Teledyne FLIR Blackfly S USB3 as the camera. The Stewart Pro is capable of Z Axis displacement between 50 - 25 mm as well as +/- 20 degrees of rotation around the X, Y and Z axes with a 50 micron position repeatability. The monitor has a resolution of 1920 x 1080 pixels as well as a pixel pitch of 265 microns. The camera is a color camera with a 25 mm focal length objective lens. It also has a frame rate of 170 frames per second and a detector resolution of 1280 x 1024 with a 4.8 micron pixel size.

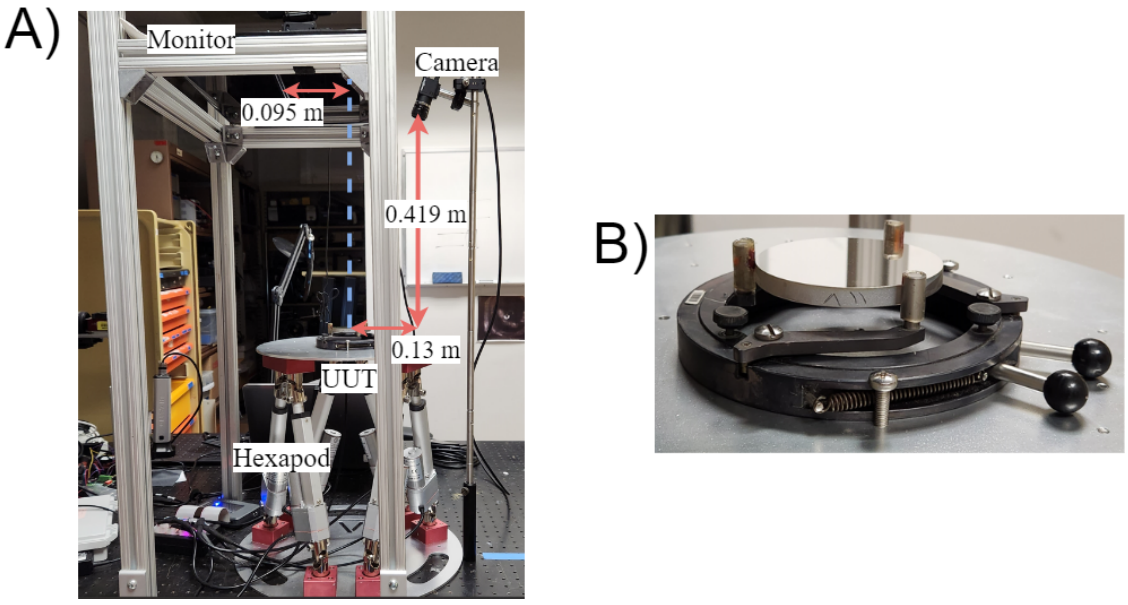

Figure 2. Photo of the multipose deflectometry setup.

2.2 Procedure

Once the deflectometry system was ready to take data, the hexapod calibration regimes were run. Afterwards, the UUT was positioned in the self-centering mount. At this point, it was important to ensure that the camera, UUT, and monitor positioning showed the full aperture of the UUT testing. The hexapod robot was adjusted to each pose and the raw measurement data was collected. After saving the raw data, we postprocessed them to generate the surface map for each pose. Finally, each surface map was fitted to the first 11 Zernike coefficients. The coefficients of each term were recorded and analyzed based on their calibration with respect to the known position. The residual values and their relationship to the intentional perturbations are shown here in Figures 3, 4, and 5.

2.3 Experimental Results

The more that the surface is moved from itsknown orientation, the more that the resultant Zernike coefficients differ from their home position values. Figure 3 shows the relationship between the measured Zernike coefficients and the stage rotation about the X-axis. Figure 4 shows the same relationship except with rotation about the Y-axis. Figure 5 shows the relationship between the resultant Zernike coefficients and the displacement of the stage in the positive Z-axis in 2 mm increments from 0 to 6 mm. The coefficients plotted were the Zernike coefficients 4 - 11. Zernike coefficients 1,2 and 3 represent Piston, X Tilt, and Y Tilt, respectively. They were not plotted because they are not shape error, but orientation changes that we intentionally produce. As shown in Figures 6 and 7, surface maps based on the residual values were generated in order to visualize the differences in the measurement result caused by the change of pose.

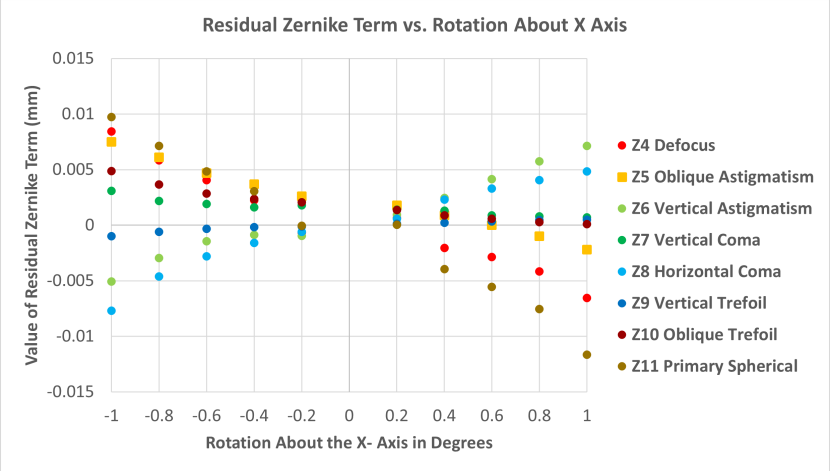

Figure 3. Plot of residuals of Zernike coefficients vs. amount of Hexapod rotation about the X Axis in degrees.

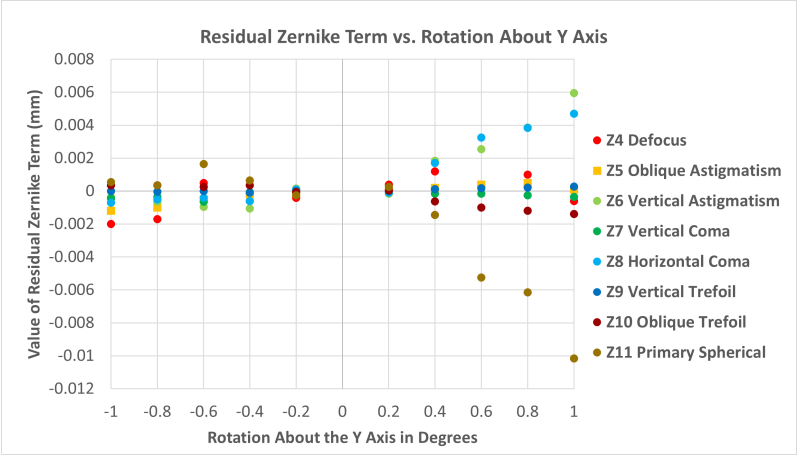

Figure 4. Plot of residuals of Zernike coefficients vs. amount of Hexapod rotation about the Y Axis in degrees.

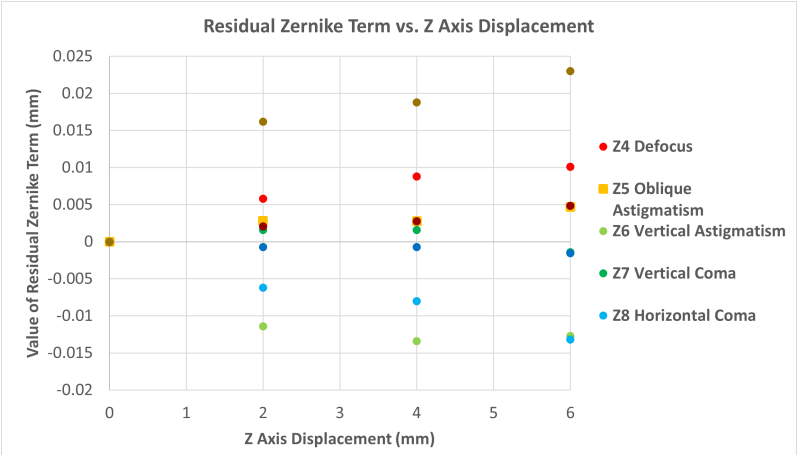

Figure 5. Plot of residuals of Zernike coefficients vs. amount of Hexapod displacement in Z Axis in mm.

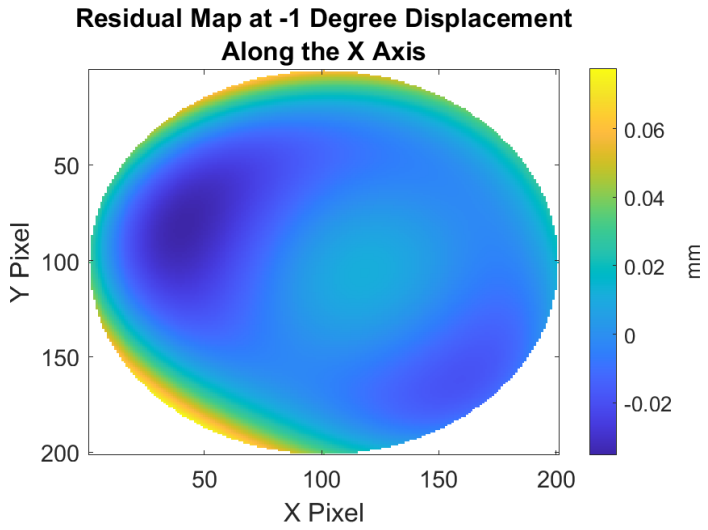

Figure 6. Map generated from Residual Zernike coefficients for -1 degree rotation about X-axis

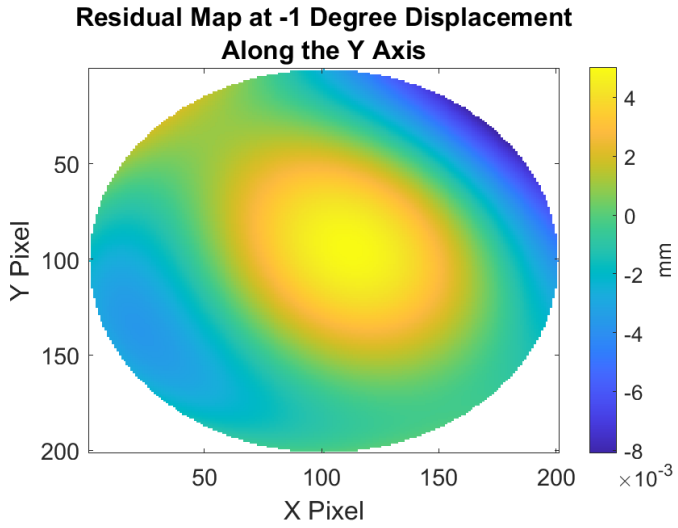

Figure 7. Map generated from Residual Zernike coefficients for -1 degree rotation about Y-axis

3. DISCUSSION

The results illustrate that even when measuring the same surface with the same deflectometry system, a user may still produce vastly different results if the UUT position and orientation differ even slightly from the pre-known pose. Furthermore, the graphs display all of the coefficients of interest on the same axes. However, when grouping the coefficients based on their radial and angular dependencies, one can see groupings in the trend patterns that would be otherwise difficult to distinguish. The following figure demonstrates the similarities between the Z4 and Z11 with rotation about the X-axis.

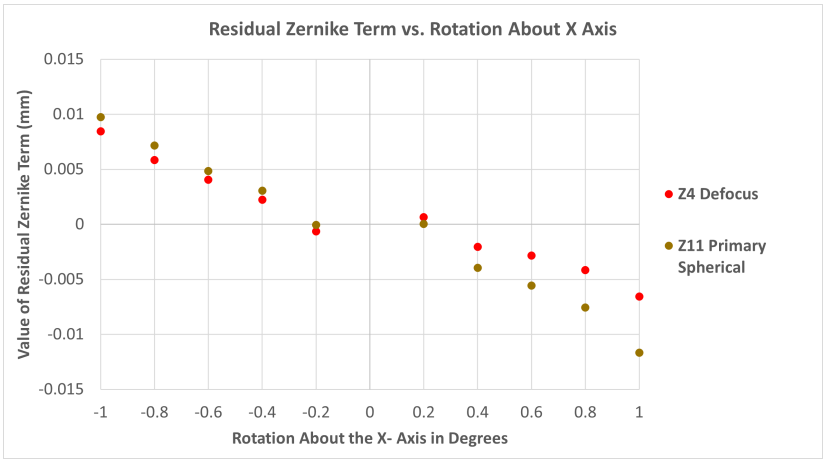

Figure 8. Zernike Term 4 and 11 trend as a function of rotation about X axis in degrees.

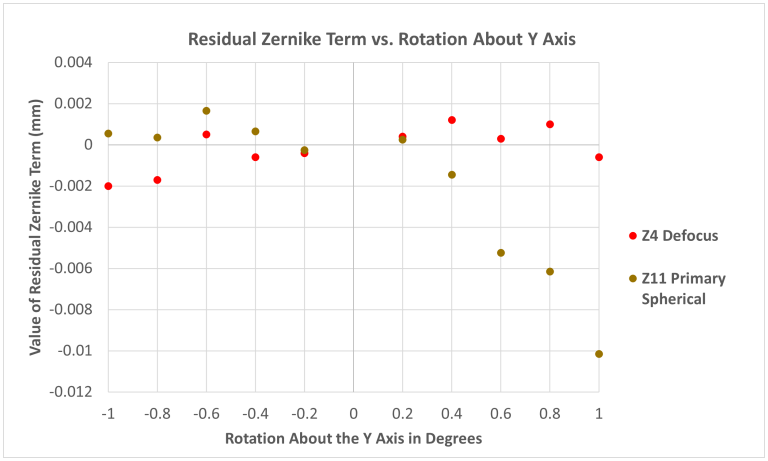

Figure 9. Zernike Term 4 and 11 trend as a function of rotation about X axis in degrees.

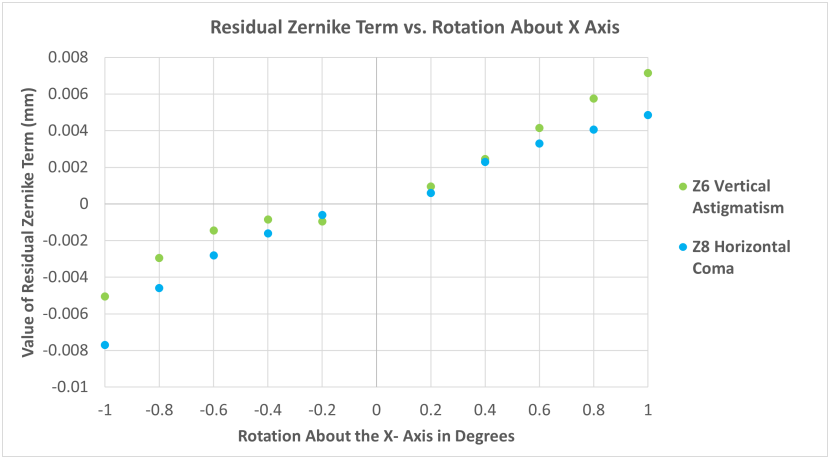

Figure 10. Zernike Term 6 and 8 trend as a function of rotation about X axis in degrees.

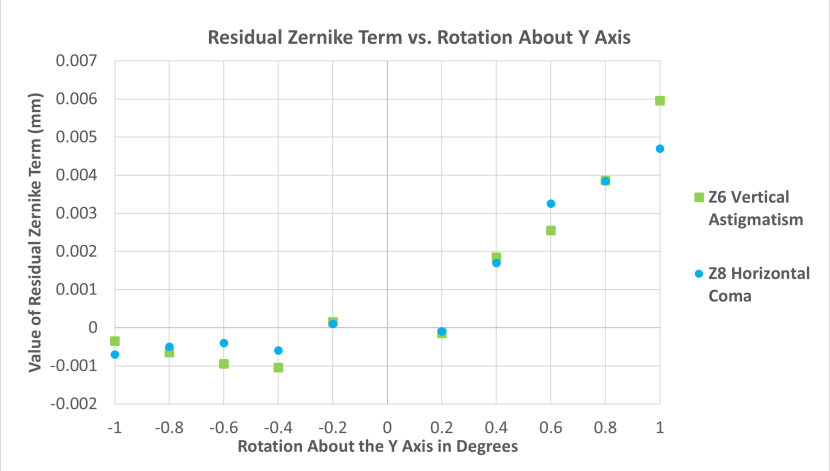

Figure 11. Zernike Term 6 and 8 trend as a function of rotation about Y axis in degrees.

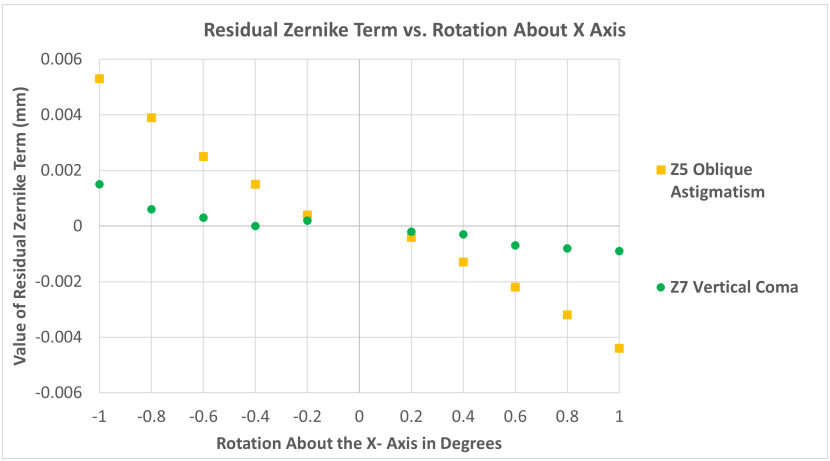

Figure 12. Zernike Term 5 and 7 trend as a function of rotation about X axis in degrees.

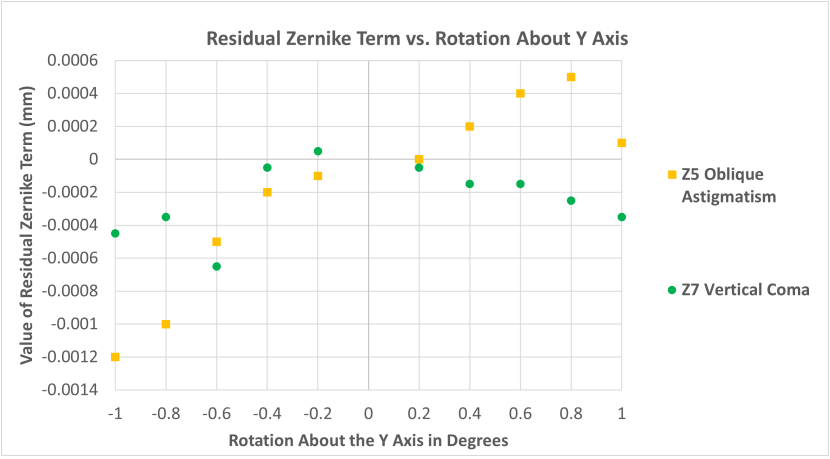

Figure 13. Zernike Term 5 and 7 trend as a function of rotation about Y axis in degrees.

Consistency in trend shape between Z4 and Z11 is expected as both terms only depend on the radial term. When these coefficients are plotted together on the same graph, their trends have a noticeably similar shape as a function of X-axis rotation. Likewise, the coefficients for Z6 and Z8 show a similar trend with regard to rotation in X-axis and rotation in Y-axis. Both terms have a cosine dependence on the angular term. This can also be seen in the coefficients for Z5 and Z7 which both have a sine dependence on the angular term.

$$Z4 = \sqrt{3}(2\rho^2 - 1) \tag{4}$$

$$Z11 = \sqrt{5}(6\rho^4 + 1) \tag{5}$$

$$Z6 = \sqrt{6}\rho^2 cos(2\theta) \tag{6}$$

$$Z8 = \sqrt{8}(3\rho^3 - 2\rho)cos(\theta) \tag{7}$$

$$Z5 = \sqrt{3}\rho^2 sin(2\theta) \tag{8}$$

$$Z7 = \sqrt{8}(3\rho^3 - 2\rho)sin(\theta) \tag{9}$$

Analysis of the Zernike coefficients' behavior as a result of their perturbations provides insight into the geometry of the system. In the relationship between Z4 and Z11 as a function of X-axis rotation, the slope of the data follows a predictable trend for rotation in both the negative and positive direction. From these observations, it was possible to conclude that the camera, UUT, and monitor system were well aligned along the X-axis since there was a nearly symmetrical impact on the Zernike coefficients with regards to rotation about the X-axis. In contrast, the system seemed to be off-axis along the Y-axis because the Zernike coefficients have a different effect when rotated in the positive Y-direction from the negative Y-direction. This can be visualized in Figure 14.

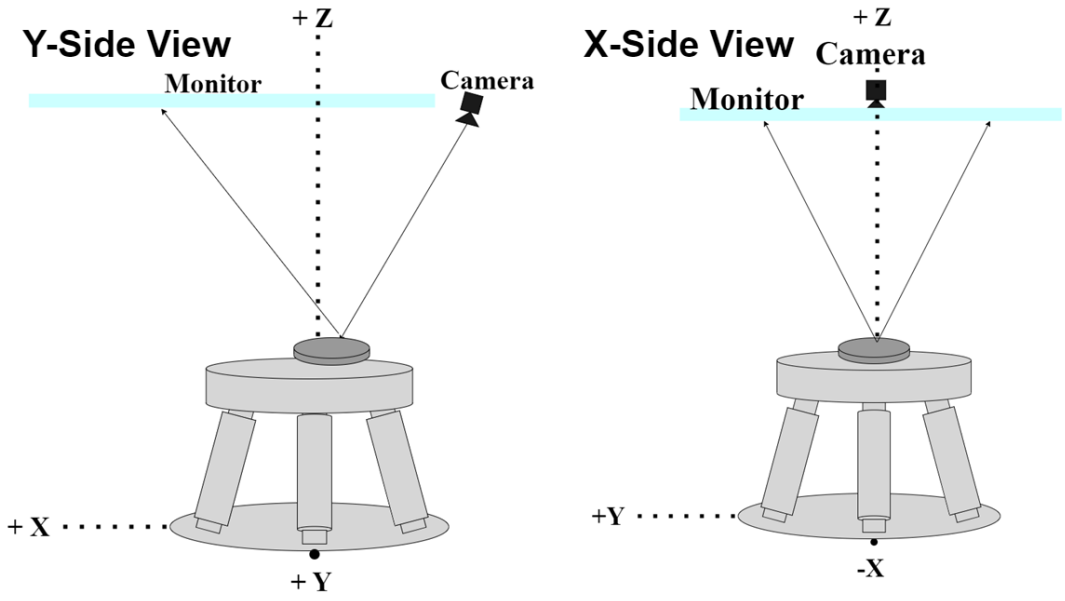

Figure 14. Schematic Diagram of system configuration on axis in X direction but off axis in Y direction.

4. CONCLUSION AND FUTURE WORKS

In conclusion, it is imperative to precisely measure the orientation and location of the UUT in a deflectometry system. Even small uncertainties in tilt about any axis or location along the Z-axis can cause noticeable differences in the measured surface map from the actual surface shape. Because many of the Zernike term vs. Perturbation trends show linearity and symmetry, future works would look into exploiting this linearity for possible benefits. One type of future research would be intentionally measuring a surface at various poses and then extracting out the true values via averaging out errors.

Another future work could explore designing a calibration regime of various poses for measuring test surfaces. This could be convenient when it is difficult to precisely determine the location and orientation of the UUT. This would be beneficial in the measurement of progressive addition lenses as well as intraocular lenses due to the delicate nature of their design. Another application where this is beneficial is measuring soft contact lenses. This is because the material is flexible enough to make each lens challenging to mount precisely. The experiment for this proceedings utilized a flat mirror, but future works would include similar experiments with spherical surfaces as well as various aspheric surfaces. Ultimately, the current findings highlight the importance of precisely understanding the orientation and location of the UUT when measuring it in a deflectometry system.

ACKNOWLEDGMENTS

This work is the result of the joint efforts of Dr. Daewook Kim, Dr. Heejoo Choi, and the late Dr. James Schwiegerling. Thank you also to the members of the Large Optics Fabrication and Testing Group and to Dr. and Mrs. Romeo and Erlinda Mercado for the generous Romeo I. and Erlinda Mercado Scholarship in Optical Sciences.

REFERENCES

[1] Schwiegerling, J. T., [*Field Guide to Visual and Ophthalmic Optics*], SPIE Press, Bellingham, WA (2004).

[2] Huang, C., Raasch, T., Yi, A., Sheedy, J. E., B.Andre, and Bullimore, M. A., "Comparison of three techniques in measuring progressive addition lenses," *Optometry and Vision Science* **89**, 1564–1573 (2012).

[3] Dubin, M. B., Su, P., and Burge, J. H., "Fizeau interferometer with spehrical reference and cgh correction for measuring large convex aspheres," *Proc. of SPIE* **7426, 74260S** (2009).

[4] Graves, L., Choi, H., Zhao, W., Oh, C., Su, P., Su, T., and Kim, D., "Model-free deflectometry for freeform optics measurement using an iterative reconstruction technique," *Opt. Let.* **43**, 2110 – 2113 (2018).

[5] Kim, D., Aftab, M., Choi, H., Graves, L., and Trumper, I., "Optical metrology systems spanning the full spatial frequency spectrum," *Frontiers in Optics (Optical Society of America)* (2016).

[6] Su, P., Parks, R. E., Wang, L., Angel, R. P., and Burge, J. H., "Software configurable optical test system: a computerized reverse hartmann test," *App. Opt.* **49**, 4404 – 4412 (2010).

[7] Smith, G., Lewis, B., Kim, D., Palmer, M., Loeff, A. R., and Burge, J., "Saguaro: Data analysis software for optical engineering," *Optical Society of America* (2012).